Optically detected magnetic resonance of Cu, Fe and Mn defects in $LiNbO_3$

2005 J. Phys.: Condens. Matter 17 6835

(http://iopscience.iop.org/0953-8984/17/43/005)

INSTITUTE OF PHYSICS PUBLISHING JOURNAL OF PHYSICS: CONDENSED MATTER

J. Phys.: Condens. Matter **17** (2005) 6835–6847 doi:10.1088/0953-8984/17/43/005

Optically detected magnetic resonance of Cu, Fe and Mn defects in $LiNbO_3$

M Pape, H-J Reyher and O F Schirmer

Fachbereich Physik, Universität Osnabrück, D-49069 Osnabrück, Germany

Received 16 August 2005, in final form 25 September 2005
Published 14 October 2005
Online at stacks.iop.org/JPhysCM/17/6835

Abstract

The optical absorptions of Cu^{2+}, Fe^{3+} and Mn^{2+} in $LiNbO_3$ are investigated using optically detected magnetic resonance (ODMR). The method is based on the changes of the magnetic circular dichroism (MCD) bands of the ions, caused by the magnetic resonances of the paramagnetic ground states of these ions. All transitions reached from the ground state of Cu^{2+} lie between 1180 and 860 nm. Three bands are observed, resulting from combined spin–orbit and trigonal field splitting of the first excited crystal field states. All features resulting from Fe^{3+} have to be ascribed to the forbidden transitions from the ^6A to the ^4G cubic precursor states. Their weak and narrow optical transitions are superimposed on the wide and strong intervalence absorption of Fe^{2+}. This ion leads to a diamagnetic contribution to the MCD, resulting from the Zeeman admixture of the first excited spin state of Fe^{2+} to its diamagnetic ground state. The MCD of Mn^{2+} is caused by an intervalence transition to the conduction band. ODMR allows us to detect these bands, lying near 400 nm, which in plain optical absorption are covered by strong precursor absorptions before the onset of the fundamental transition.

1. Introduction

The most compelling way to tie the optical properties of a paramagnetic defect to its underlying material structure is to study the corresponding optically detected magnetic resonance (ODMR). For absorption studies this consists in detecting the changes of the related magnetic circular dichroism (MCD) induced by the magnetic resonance of the ground state of the defect. The MCD is proportional to the difference between the absorptions of two polarizations of light, left and right circular with respect to the direction of the magnetic field. In this ODMR scheme, the magnetic resonance, containing information on the structure of the defect, is monitored by changes of the MCD, containing information on the optical bands involved in the absorption process.

Information about defect-induced absorption processes is necessary, e.g., if one wants to assess the influence of a defect on the performance of a photorefractive material. $LiNbO_3$

(LN) is one of the most important among such compounds; also, its wide range of electro-optic, acousto-optic etc properties qualifies the material for further applications, in which light induced defect excitations can play a role.

Previously, the main intrinsic paramagnetic lattice perturbation in LN, the Nb_{Li}^{4+} antisite defect, as well as the Ti_{Li}^{3+} ion, were studied by the indicated ODMR method [1]. In this way the related intense optical absorptions could consistently be explained by intervalence transitions of the Nb_{Li}^{4+} and the Ti_{Li}^{3+} electrons to the neighbouring Nb_{Nb}^{5+} conduction-like states. In the present contribution the optical absorption properties of the extrinsic defects Cu^{2+}, Fe^{3+} and Mn^{2+} will be treated. The investigations will also shed some light on the the MCD properties of Fe^{2+}. These dopings have considerable importance for the photorefractive operation of LN [2–6], and detailed knowledge about their absorption properties is thus essential.

The ODMR(MCD) investigations will identify the wavelength regions in which the indicated ions have their optical absorptions, e.g. in LN. This will allow us to interpret at least a part of the total absorption of a compound, which usually also arises from further optically active charge states of the doping as well as of other extrinsic or intrinsic defects. Furthermore, the extra optical information conveyed by the MCD spectra, as compared to plain optical absorption bands, permits a more detailed spectroscopic analysis, especially of the excited states involved in the relevant optical transitions.

2. Essentials of ODMR monitored by changes of the MCD

The MCD, being a special case of a circular dichroism (CD), is proportional to the differential absorbance, $\Delta\alpha = \alpha_+ - \alpha_-$, presented by a sample for left- and right-polarized light propagating along the direction of an applied static magnetic field B (see, e.g., figure 3). This means that

$$\Delta\alpha \propto (|\langle F|x + \mathrm{i}y|I\rangle|^2 - |\langle F|x - \mathrm{i}y|I\rangle|^2), \tag{1}$$

if, for illustration, only a single transition from a ground state $|I\rangle$ to an excited state $|F\rangle$ is considered, induced by transition operators $x \pm \mathrm{i}y$ for left and right circularly polarized light, respectively. For further details, see e.g. [7, 8]. In non-cubic samples a pure MCD can usually only be recorded if B coincides with an axis of the material. Otherwise, the observed signal will be influenced by the linear dichroism (LD), and the contributions of MCD and LD are difficult to disentangle [9]. All MCD measurements on LN are therefore performed for $B \parallel c$. The MCD signal associated with an isolated electronic transition contains two main contributions: $\mathrm{MCD} = \mathrm{MCD}_{\mathrm{dia}} + \mathrm{MCD}_{\mathrm{para}}$. The *diamagnetic* term $\mathrm{MCD}_{\mathrm{dia}}$, present also for defects with diamagnetic ground states, results from the B-induced shift between the initial and final optical states or from the B-induced mixture between neighbouring levels. An example for the latter phenomenon will be given in section 4.2.

In paramagnetic systems at low temperatures the *paramagnetic* term $\mathrm{MCD}_{\mathrm{para}}$ dominates; it is proportional to the population difference of the Zeeman levels of the ground state. For the special case of $S = 1/2$ this is

$$\Delta n = n_0 \tanh(\mu_{\mathrm{B}} g B/(2kT)) \tag{2}$$

(n_0, defect density; μ_{B}, Bohr magneton; g, g-value; T, temperature). The present paper will mainly be concerned with this paramagnetic term. In order to increase the sensitivity and to avoid noise created by He bubbles, the measurements are usually performed at superfluid helium temperatures, $T \approx 2$ K.

The MCD of broad optical absorptions in the solid state is composed by the same bands [7] as the corresponding optical absorption function, $\alpha(E)$:

$$\mathrm{MCD}(E) \propto \sum c_i f_i(E), \qquad \alpha(E) \propto \sum d_i f_i(E). \tag{3}$$

Here, the $f_i(E)$ are the shape functions, identical in both cases; the coefficients d_i all have a positive sign, describing a constructive superposition of the component bands in absorption, whereas the c_i can differ in sign, since MCD is a difference spectroscopy. In comparison to optical absorption, MCD spectra thus offer the advantage of higher resolution. In order to identify the band positions, in the MCD spectra the energies of both the positive as well as the negative extrema of the MCD pattern must be determined.

The ODMR(MCD) method is a double resonance technique, detecting the combined influence of optical and microwave photons, having energies E and $h\nu$ respectively, on the investigated system. Because of the condition for magnetic resonance, $h\nu = \mu_B g B$ in its most simple form, a change of $h\nu$ is equivalent to a variation of B. In an experiment either (i) the optical energy E is fixed and B is varied, then one arrives at the MCD(B) spectrum, which includes those values of B where a resonance occurs, if a non-zero microwave field is applied, or, alternatively, (ii) B is fixed at such a resonance value and the optical energy is varied. This is performed under non-zero as well as zero microwave fields, i.e. under the conditions of resonance and no resonance. The difference between the two measurements is the so-called *tagged* MCD(E) [8]. It collects those contributions to the total MCD which arise from that specific defect, whose ground state is affected by the resonance. All further defects, possibly adding their contributions to the total MCD, are excluded from MCD(E), because they do not contribute to the resonance. As already mentioned above, there can be polarization phenomena influencing the experimentally detected signal even for $B = 0$ [9]; usually such background spectra are subtracted from the experimental raw data. This leads to the 'corrected' MCD; if not qualified differently, all spectra labelled MCD in the following will be such corrected versions.

Summarizing, we state that in addition to its main advantage, the logically most compelling assignment of optical absorption bands to a defect structure, a great asset of the ODMR(MCD) method is its ability to detect exactly that absorption belonging to a definite defect among a superposition of several bands of different origin. Furthermore, being a difference method, the observation of ODMR(MCD) enhances the resolution as compared to plain absorption, where the component bands are adding to each other to yield the total absorption.

3. Experimental details

The ODMR set-up is of standard type, as described, e.g., by [8]. It consists of a spectrometer for circular polarization measured at low temperatures along the direction of a B field of up to 3 T produced by a superconducting magnet. The sample can be exposed to microwave fields emanating from an open waveguide, having the optional frequencies 9, 34 and 70 GHz.

The following LN specimens were investigated: nearly stoichiometric material (Li fraction of 49.9%) doped with Cu, congruently melting material (48.4%) doped with Fe and stoichiometric material (50.0%) containing Mn and Fe. Previous assignments of the EPR spectra of the ions Cu^{2+}, Fe^{3+} and Mn^{2+}, observed with the samples, indicate that the ions in all cases are incorporated at Li sites of the LN lattice.

4. ODMR and MCD of Cu^{2+}, Fe^{3+} and Mn^{2+} in $LiNbO_3$

4.1. Cu^{2+} ($3d^9$)

Figure 1 shows the ODMR of Cu-doped LN. With increasing B the MCD is seen to rise according to equation (2), except for a sharp dip, representing a resonance, at 1113 mT. Under the applied microwave frequency, $\nu = 34.83$ GHz, this corresponds to a g-value, measured

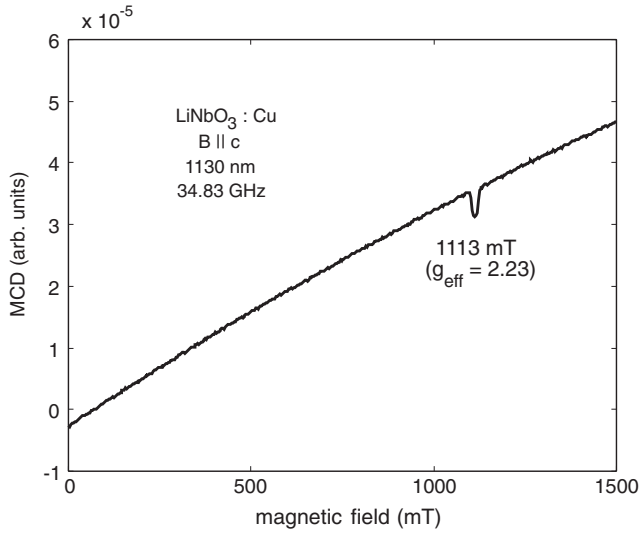

Figure 1. Optically detected magnetic resonance of Cu-doped $LiNbO_3$. The dip represents the decrease of the MCD, measured at 1130 nm, which is caused by the decrease of the population difference of the $S = 1/2$ ground-state sublevels in figure 3 under resonance.

along the c-axis of LN, of $g_c = 2.23$ according to the resonance condition $h\nu = \mu_B g B$. This is consistent with the fact that the signal arises from Cu^{2+}_{Li}; this g-value was identified by Corradi *et al* [10] in their EPR study of LN:Cu^{2+} when B was pointing along the c-axis of the crystal. EPR signals of Cu are usually characterized by the typical hyperfine splitting of the corresponding signals into four lines; the two stable isotopes of Cu, ^{63}Cu and ^{65}Cu, both have a nuclear spin $I = 3/2$ and nearly identical nuclear magnetic moments. That such structures are not observed does not argue against the assignment to Cu^{2+}: for experimental reasons the scanning of B had to occur in rather coarse steps, limiting the obtainable resolution. Furthermore, for some unknown reason ODMR spectra tend to be wider than the corresponding EPR signals.

The identification of the ODMR signal of Cu^{2+} (figure 1) opens the opportunity to find the connected MCD changes, being related to the corresponding optical absorption. In figure 2 the MCD of Cu^{2+} is seen, tagged by this resonance. Three extremal MCD changes, two with positive and one with negative sign, appear, labelled by the related peak wavelengths. They define the peak positions of the bands contributing to the MCD.

These values are typical for the lowest crystal field transitions of Cu^{2+}, suggesting that the relevant absorption bands are caused by such transitions between the E ground state of Cu^{2+} and the excited T_2 states (in O_h symmetry, left of figure 3), split by the trigonal crystal field, symmetry C_3[1] (middle of figure 3). Coupling the orbitals to the $S = 1/2$ spin leads to the levels shown on the right. The excited states split into three levels by the combined action of spin–orbit coupling and trigonal field. This leads to the observed three transitions. Two of them are connected with a positive MCD and one with a negative one. This assertion is based on the group theoretical designations indicated by the boxes representing the excited states. Under application of the magnetic field the levels split, shown for the ground state in detail.

[1] It should be noted that the ground state of Cu^{2+} in LN rather has C_1 symmetry, caused by a static Jahn–Teller effect [9]. Still, the analysis of the MCD is based on C_3 since the optical transitions are mainly influenced by the cubic and trigonal components of the crystal field.

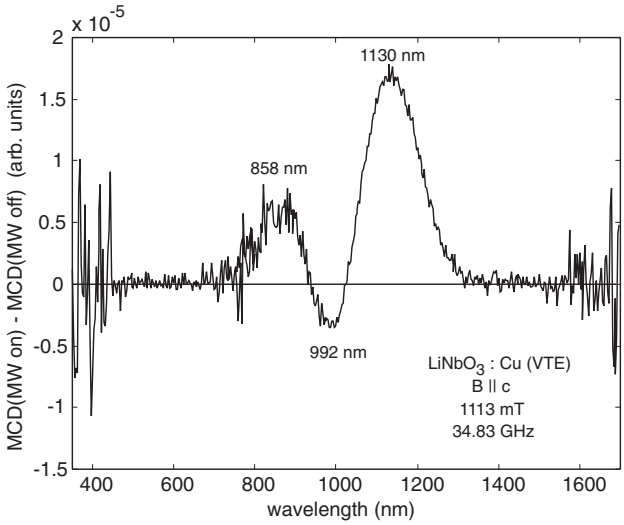

Figure 2. Tagged MCD spectrum of Cu^{2+} in $LiNbO_3$. True spectra are shown, characterized by detector noise.

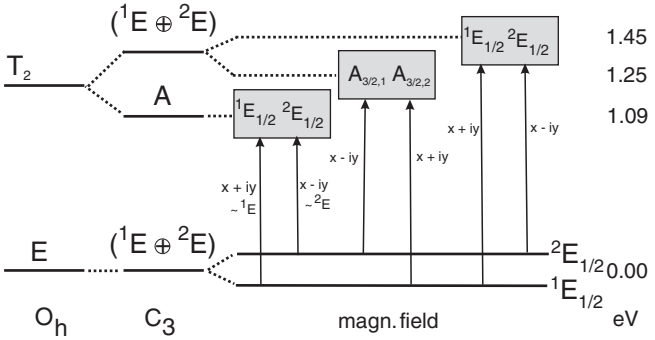

Figure 3. Level scheme of Cu^{2+} in an octahedral (O_h) and a trigonal (C_3) crystal field under an applied magnetic field. The levels are labelled by their C_3 group theoretical symbols according to [11]. On the right the levels resulting from coupling a spin 1/2 to the orbitals in the C_3 column on the left are given. The designation of the excited states is represented by the boxes. The vertical arrows indicate the transitions induced by left $(x + iy)$ and right $(x - iy)$ circularly polarized light, transforming as ^1E and ^2E, respectively, based on the group theoretical selection rules. ODMR is observed by changing the relative populations of the ground-state Zeeman levels under resonance.

The corresponding sublevels transform as $^1E_{1/2}$ and $^2E_{1/2}$ in C_3, if originating from coupling to an orbital A singlet state, or as two $A_{3/2}$ states, if resulting from coupling to an orbital E doublet state [11]. The symmetry based theoretical selection rules show which transitions are allowed for left- $(x + iy)$ and right-$(x - iy)$ polarized light, transforming as ^1E and ^2E, respectively. It is seen that three pairs of left/right-polarized absorptions can occur. Two of them predict a positive $\Delta\alpha$ and one a negative $\Delta\alpha$. This coincides with the observation shown in figure 2. They reflect the spin–orbit/trigonal crystal field structure of the excited states and the related crystal field transition energies of Cu^{2+} in LN.

No further optical transitions starting in the E ground state of Cu^{2+} are observed. Therefore, the features in figure 2 represent the total optical absorption related to Cu^{2+}. With Cu-doped

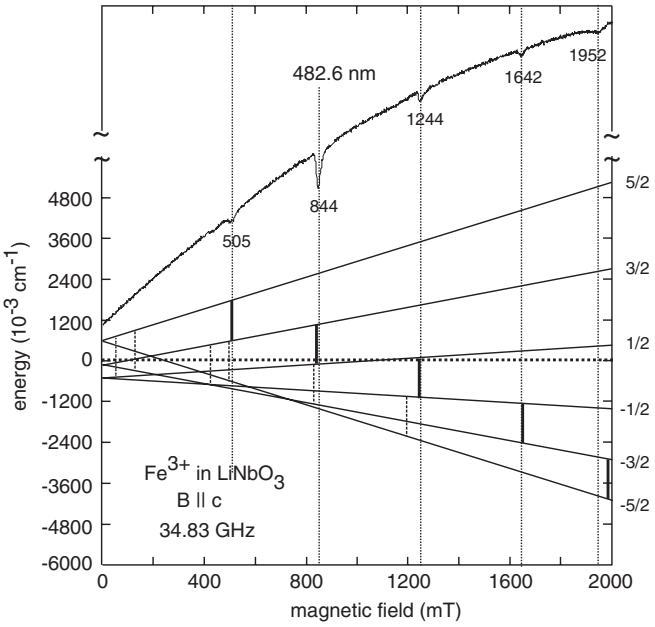

Figure 4. Upper part: ODMR of the five allowed $|\Delta m_s| = 1$ transitions for Fe^{3+} in $LiNbO_3$, monitored by resonance-induced changes of the MCD at 482.6 nm. Lower part: comparison with predicted transitions derived from the Hamiltonian and parameters given in the text. The allowed transitions are presented by full vertical lines, the forbidden ones by dashed lines.

LN usually further Cu-induced transitions are observed, starting at about 2 eV and extending up to the fundamental absorption edge, about 3.7 eV [12]. They arise from the diamagnetic charge state Cu^+ [2, 4], corresponding to a full 3d shell. Both charge states together decisively determine the photorefractive behaviour of LN:Cu [2, 3].

4.2. Fe^{3+} ($3d^5$)

There are various EPR studies of isolated Fe^{3+}_{Li} in LN performed at room temperature [13–17]. At the Li site, this ion occupies an axial position and the spectra can be modelled by the Hamiltonian, consistent with the prevailing C_3 symmetry,

$$H = \mu_B \mathrm{BgS} + b_2^0 O_2^0 + b_4^0 O_4^0 + b_4^3 O_4^3 + c_4^3 \Omega_4^3 \tag{4}$$

which operates on the spin-only $S = 5/2$ ground-state manifold, with an axially symmetric g-tensor and the irreducible tensor operators [18] O_k^q and Ω_k^q. The following parameter values were identified at 25 K [19] for Fe^{3+}_{Li}: $g_{zz} = 2.019$, $g_{xx} = 1.983$, $b_2^0 = 0.1768\ \mathrm{cm}^{-1}$, $b_4^0 = -0.0049\ \mathrm{cm}^{-1}$, $b_4^3 = 0.0650\ \mathrm{cm}^{-1}$, $c_4^3 = -0.0380\ \mathrm{cm}^{-1}$. On this basis the resonances investigated by the present ODMR study (figure 4) also prove the presence of isolated Fe^{3+}_{Li}, since the accessible parameters in this study, limited to $B \parallel c$, have identical or nearly identical values: $g_{zz} = 2.019$, $g_{xx} = 1.983$, $b_2^0 = 0.1740\ \mathrm{cm}^{-1}$, $b_4^0 = -0.0040\ \mathrm{cm}^{-1}$. The difference in the latter two parameters with respect to those determined by EPR [19] might be attributed to the fact that the present ones were obtained at a lower temperature, 2 K.

As an introduction to the structure of the related MCD spectra, figure 5 shows the optical absorption of congruent LN, doped with Fe. The various features, marked by arrows, are commonly interpreted as in table 1.

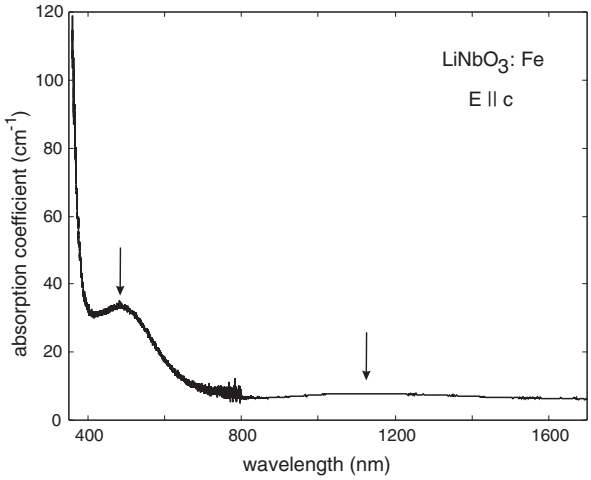

Figure 5. Absorption spectrum of Fe-doped $LiNbO_3$. The arrow at 1160 nm marks the crystal field transition of Fe^{2+}. The left arrow points to the sharp spin-forbidden transition in Fe^{3+}; it is superimposed on the wide intervalence transition absorption of Fe^{2+} to the conduction band.

Table 1. Absorption bands in $LiNbO_3$:Fe and their assignment according to Clark *et al* [20].

Band	Assignment
1.1 eV/1127 nm	Crystal field transition T_2–E of Fe^{2+}
2.6 eV/477 nm	Intervalence transfer transition Fe^{2+}–Nb^{5+}
2.55 eV/486.2 nm	Spin-forbidden transitions of Fe^{3+}
2.95 eV/420.3 nm	

The corresponding MCD spectra of LN:Fe are seen in figure 6. They comprise various nearly parallel curves, which were obtained at a series of different B fields, rising from 250 to 3000 mT in steps of 250 mT. The inset shows that, depending on the studied wavelength, two types of B-dependence can be discriminated. In some regions, such as at $\lambda = 388$ nm, the MCD changes linearly with B, whereas at, e.g., 422 nm, a nonlinear approach to a saturation value at high B is seen. Later it will be shown that the first type of behaviour is caused by a diamagnetic MCD originating from Fe^{2+}, while the second one is due to the paramagnetism of the ground state of Fe^{3+}. The latter is demonstrated by plotting the MCD of Fe^{3+} (figure 7), 'tagged' by the resonance at 844 mT in figure 4, i.e. by the wavelength dependence of the MCD changes which are caused by this resonance of Fe^{3+}. This selects only Fe^{3+} contributions and thus there are zero MCD changes, for instance at 388 nm, where Fe^{2+} contributions occur in the spectra of the total MCD (figure 6); see also the next paragraph.

These assignments follow the interpretation of the absorption spectra (figure 5), as given in table 1, which indicate that also in optical absorption there is a superposition of Fe^{2+} and Fe^{3+} features. The latter ones, in figure 5 causing only the sharp little spin-forbidden peak marked by an arrow, lead to the structures in figures 6 and 7 near 483 nm. The further Fe^{3+}-related features near 414 nm and below in figures 6 and 7 are covered by the strong rise in absorption near 400 nm in the absorption spectrum (figure 5) and are recovered only by the selectivity of the MCD technique. The Fe^{2+} ion, in optical absorption (figure 5) causing the wide intervalence transfer band peaked near 500 nm, influences the MCD spectra (figure 6) by its specific diamagnetic MCD of the ground state. This is absent in the tagged MCD of Fe^{3+} (figure 7), where contributions from the Fe^{2+} ground state are not collected.

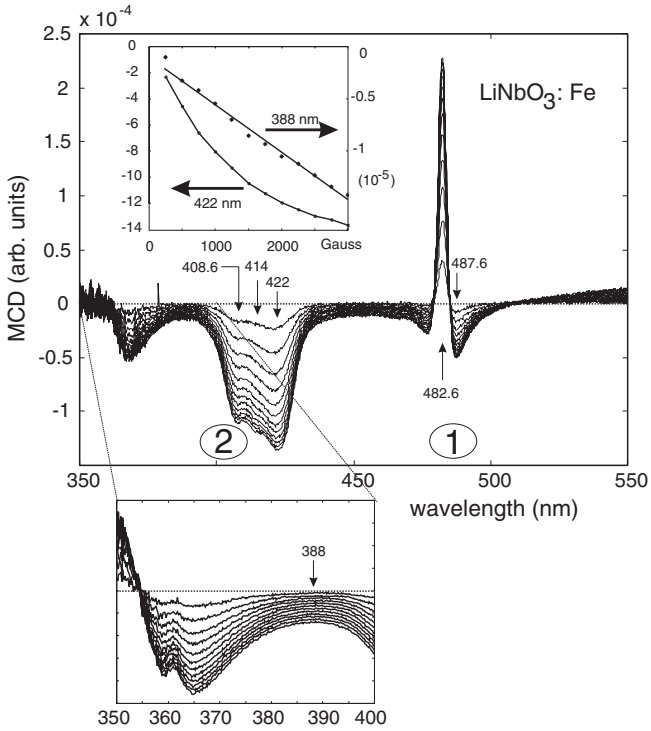

Figure 6. MCD spectra of $LiNbO_3$:Fe at B between 250 and 3000 mT, varied in steps of 250 mT. The inset shows the MCD signal heights as depending on B. The diamagnetic parts change linearly with B, the paramagnetic ones non-linearly. It should be noted that the angle between c and B was about 0.5°. Compare with figure 10, where the angle was carefully set to 0°.

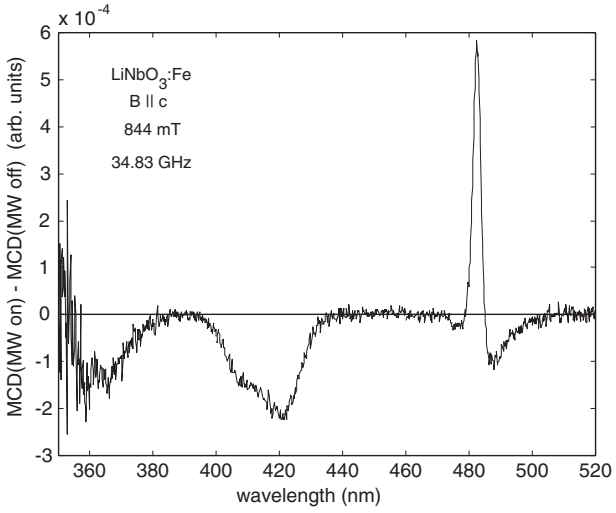

Figure 7. Tagged MCD of Fe^{3+} in $LiNbO_3$.

In order to analyse the origin of the Fe^{3+}-related phenomena, previous knowledge about the corresponding spin-forbidden transitions and excited state levels in Al_2O_3:Fe^{3+}, almost

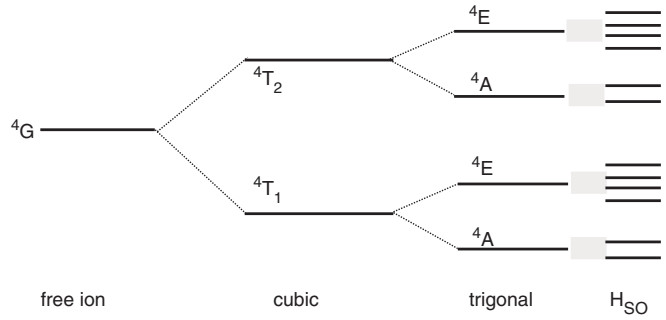

Figure 8. Level scheme expected for the excited states of Fe^{3+}, derived from the ^4G orbital state of the free ion by incorporation into a cubic and a trigonal crystal field and by spin–orbit coupling.

isostructural to LN:Fe^{3+}, is used [21], since no relevant information about Fe^{3+} in LN is available so far. In the crystal field study of [21] the first excited states, reached by photons from the $^6A_1$ ground state, are those shown in figure 8. It is expected that the group of bands near 483 nm (region 1) has to be attributed to the sublevels originating from the $^4T_1$ precursor of the cubic situation and those near 414 nm (region 2) to those originating from $^4T_2$. We concentrate our attention on these two types of transition. The trigonal part of the crystal field and spin–orbit coupling lead to the six spin–orbit sublevels for each of the ^4T_i orbital states indicated in figure 8. For Al_2O_3:Fe^{3+} the splitting between the $^4T_1$ and $^4T_2$ levels has been found to be larger than the trigonal and spin–orbit energy changes, the same is expected for LN:Fe^{3+}. This predicts the observed bunching of the relevant MCD transitions into regions 1 and 2 (figure 6). The widths of the MCD spectra in each of these regions should be given by the trigonal field splittings, found to be larger than the spin–orbit effects [21]. For a more detailed discussion of the Fe^{3+} MCD spectra [22] can be consulted.

4.3. Fe^{2+} ($3d^6$)

This charge state of isolated iron in congruent LN has been studied previously by Juppe *et al* [23] using thermally detected electron paramagnetic resonance (TDEPR). It was ascertained that the ground state has a spin $S = 2$, expected for the case where Hund's rules are not broken in the $3d^6$ system. Figure 9 shows the level scheme [24] by which the TDEPR results were interpreted. The observed resonances arise from the first excited state, spin projections $|m_S| = 1$, lying 15–20 cm^{-1} above the diamagnetic ground state, $|m_S| = 0$. There is a slight population of the excited state at 6 K, the temperature of the TDEPR measurements [23]. In the ODMR experiments the temperature is much lower, $T = 2$ K, and thus the diamagnetism of the ground state determines the behaviour of the system. It turns out that it offers an ideal example of a *diamagnetic* MCD.

In the present case the B-dependence of the MCD is expected to be caused by the Zeeman admixture, A_{Zee}, of the first excited state, to the ground state,

$$A_{Zee} = \langle 0|\mu_B g_{xx} B_x S_x|\pm 1\rangle/(E_0 - E \pm 1). \tag{5}$$

Here it is considered that spin selection rules lead to a finite matrix element only for spin transitions perpendicular to B, which is oriented parallel to c (see above). It is seen that the admixture is linearly proportional to B, explaining the B-dependence in the inset of figure 6. Also the dependence on the direction of the magnetic field, implied by equation (5), is borne

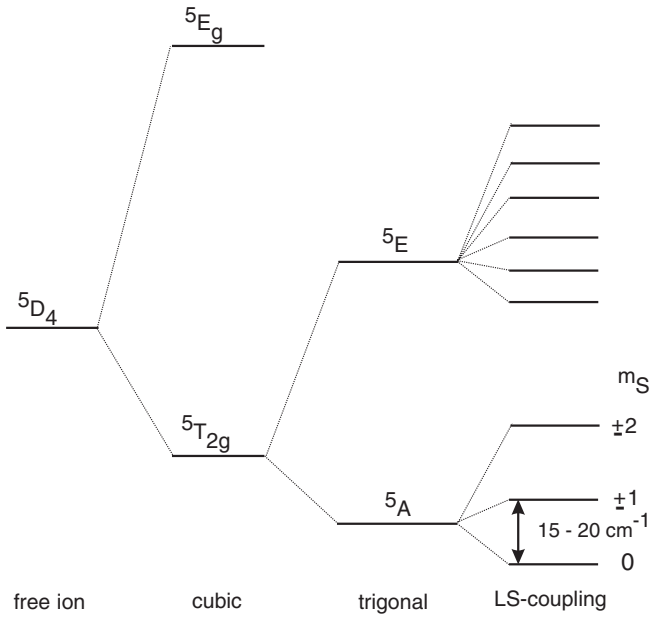

Figure 9. Level structure of Fe^{2+} in $LiNbO_3$.

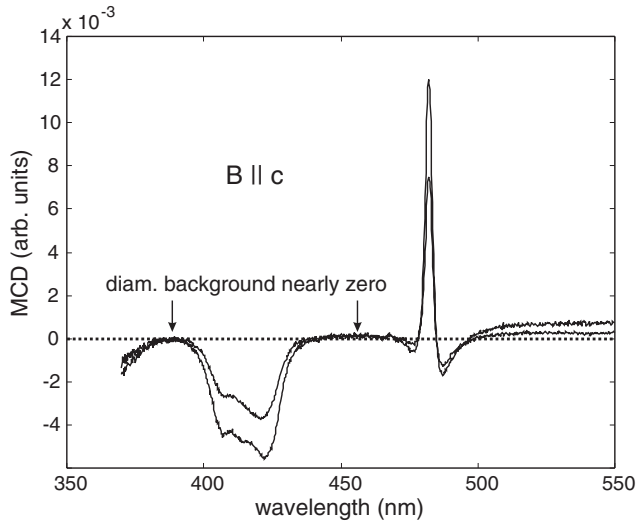

Figure 10. MCD of $LiNbO_3$:Fe for B aligned along c. No MCD is observed at the wavelengths indicated by arrows, in contrast to the corresponding measurements of figure 6, where the angle between B and c was about 0.5°.

out by the experiment: for B parallel to the trigonal axis of LN, among the shown total MCD the diamagnetic MCD contributions of Fe^{2+} vanish (figure 10). This is observed in the total MCD spectra of figure 6, where there is a slight misalignment of B from the c-axis by about 0.5°.

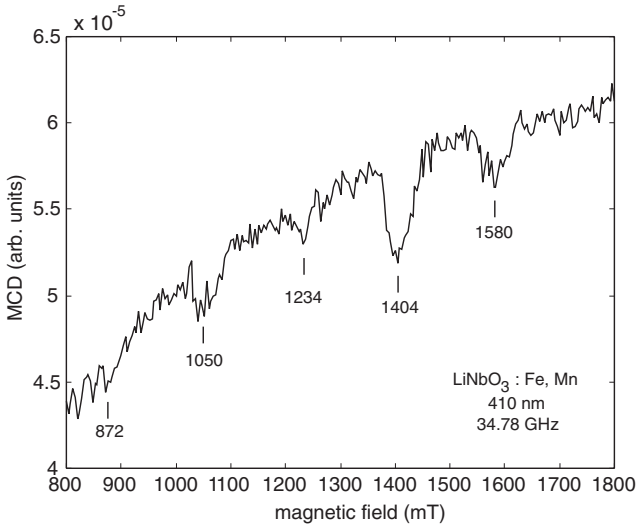

Figure 11. ODMR of Mn^{2+} in $LiNbO_3$. Five transitions are observed, as expected and found, in analogy to the isoelectronic Fe^{3+}; see figure 4.

4.4. Mn^{2+} ($3d^5$)

This ion is isoelectronic to Fe^{3+}, and thus ODMR spectra as in figure 11 are expected and found, analogous to those of Fe^{3+} in figure 4. Here the detected resonances are observed at the fields predicted from a previous EPR analysis of LN:Mn^{2+}_{Li} [25]. In these studies also the hyperfine interactions characteristic for Mn^{2+} EPR spectra, caused by the only stable Mn isotope (100%, $I = 5/2$) have been determined. They lead to sizeable splittings of about 8 mT. Accordingly, the components of the ODMR spectra of Mn^{2+} are wider than for Fe^{3+} (figure 4). The hyperfine splittings, however, could not be resolved, as usual for ODMR spectra.

The tagged MCD spectra of LN:Mn^{2+} are shown in figure 12. They are composed of two bands with extrema at 398 and 410 nm. In the case of the isoelectronic Fe^{3+} ($3d^5$) transitions in this range are dominated by weak spin-forbidden transitions to the excited quartet states. Apparently, the strongest excitations arising from Mn^{2+} ($3d^5$) are caused by a different mechanism. The following model can explain the findings. By absorbing a photon, an intervalence transfer process can excite an electron from Mn^{2+} to the conduction band. An analogous process is known to occur only for Fe^{2+} and not for Fe^{3+}. For Fe^{2+}, however, such an excitation cannot be monitored by MCD, because there is no paramagnetic MCD for Fe^{2+}; the diamagnetic MCD identified for Fe^{2+} is not sensitive to a resonance phenomenon and cannot, therefore, be connected to the responsible defect by tagging. This, however, is possible for an intervalence transfer transition from Mn^{2+} to the conduction band, since here the ground state is the paramagnetic Mn^{2+}, identifiable by its ODMR. The comparatively high oscillator strength of the intervalence transfer transitions of Mn^{2+} probably prevents the detection of the weak spin-forbidden MCD features.

The given interpretation of the identified tagged MCD bands as reflecting at least part of the intervalence transitions of Mn^{2+} is supported by the observation that illumination into the Mn^{2+} bands leads to a photorefractive effect, resulting from photoconductivity induced by absorption of Mn^{2+} [26, 6]. The photoconductivity is triggered by a wide band [26], having a similar low energy onset as the one in figure 12. Since the present investigations were made at the low temperature of 2 K, the detected bands may be more narrow than those leading

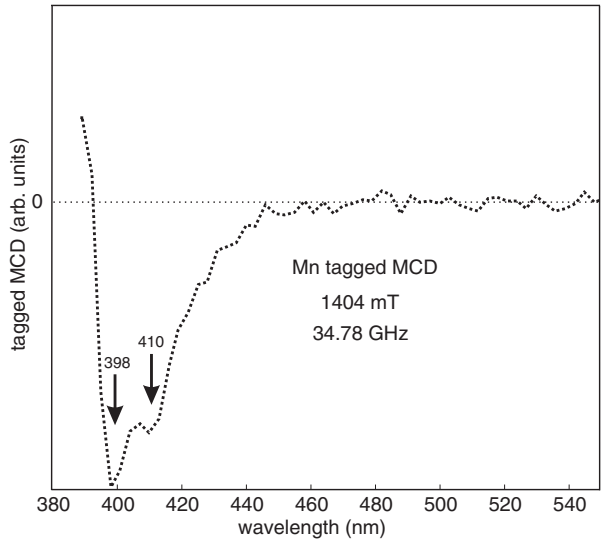

Figure 12. Tagged MCD of Mn^{2+} in $LiNbO_3$.

to photoconductivity, studied at room temperature. This can explain why photorefractivity is observed by Mn^{2+} at 458 nm [6], which is only near the onset of the band in figure 12. In the absorption spectra of LN:Mn usually a further strong absorption band with peak at 577 nm is observed, rising in intensity, when the specimen is oxidized [6]. This has to be attributed to Mn^{3+}; the band is probably caused by a charge transfer transition from the valence band to this charge state. The ground state of Mn^{3+} is likely to be diamagnetic, preventing the observation of ODMR.

5. Conclusions

The presented investigations of the optical absorption of LN containing Cu, Fe and Mn have definitely identified the wavelength regions in which optical transitions originating in the ground states of Cu^{2+}, Fe^{3+} and Mn^{2+} occur. The ODMR(MCD) method has furthermore allowed us to obtain information on the structure of the involved levels and on the optical excitation mechanisms.

Of course, ODMR(MCD) can essentially only be used for ions with paramagnetic ground states. It fails for the numerous ions not in this category. Their optical bands must be identified as well, if one wants to fully understand the optical absorption properties of a compound, necessary for instance for unravelling the charge transfer phenomena involved in the photorefractive behaviour of a material. Here a complementary method can be employed, which makes use of the simultaneous registration of light-induced changes of optical absorption and EPR spectra. By a self-consistent interpretation of these data also absorption phenomena which are connected to diamagnetic ground states can be labelled (see e.g. [27]). Also the complete charge transfer paths triggered by photon absorption can be reconstructed.

References

[1] Reyher H-J, Schulz R and Thiemann O 1994 *Phys. Rev.* B **50** 3609
[2] Imbrock J, Wirp A, Kip D, Krätzig E and Berben D 2002 *J. Opt. Soc. Am.* B **18** 1822

[3] Hartwig U, Peithmann K, Sturman B and Buse K 2005 *Appl. Phys.* B **80** 227
[4] Krätzig E and Orlowski R 1978 *Appl. Phys.* **15** 133
[5] Buse K, Adibi A and Psaltis D 1998 *Nature* **393** 665
[6] Yang Y, Psaltis D, Luennemann M, Berben D, Hartwig U and Buse K 2003 *J. Opt. Soc. Am.* B **20** 1491
[7] Stephens P J 1976 *Adv. Chem. Phys.* **25** 197
[8] Spaeth J M, Niklas J R and Bartram R H 1992 *Structural Analysis of Point Defects in Crystals* (Berlin: Springer)
[9] Jensen H P, Schellman J A and Troxell T 1978 *Appl. Spectrosc.* **32** 192
[10] Corradi G, Polgar K, Bugai A A, Zaritskii I M, Rakitina L G, Grachev V G and Deryugina N I 1978 *Sov. Phys.—Solid State* **28** 412
[11] Altmann S L and Herzig P 1994 *Point Group Theory Tables* (Oxford: Clarendon)
[12] Räuber A 1978 *Current Topics in Materials Sciences* vol 1, ed E Kaldis (Amsterdam: North-Holland) p 481
[13] Towner H H, Kim Y M and Story H S 1972 *J. Chem. Phys.* **56** 3676
[14] Herrington J, Dischler B and Schneider J 1972 *Solid State Commun.* **10** 509
[15] Mehran F and Scott B A 1972 *Solid State Commun.* **11** 15
[16] Malovichko G I and Grachev V G 1985 *Sov. Phys.—Solid State* **27** 1678
[17] Grachev V G and Malovichko G I 1985 *Sov. Phys.—Solid State* **27** 443
[18] Altshuler S A and Kozyrev B M 1974 *Electron Paramagnetic Resonance in Compounds of Transition Metals* (New York: Wiley)
[19] Malovichko G I, Grachev V G, Schirmer O F and Faust B 1993 *J. Phys.: Condens. Matter* **5** 3971
[20] Clark M G, DiSalvo F J, Glass A M and Peterson G E 1973 *J. Chem. Phys.* **59** 6209
[21] Eigenmann K, Kurtz K and Günthard H H 1972 *Chem. Phys. Lett.* **13** 54
[22] Pape M 2004 *Doctoral Thesis* University of Osnabrück
[23] Juppe S and Schirmer O F 1990 *Solid State Commun.* **76** 299
[24] Meshcheryakov V F, Grechushnikov B N and Kalinkina I N 1974 *Sov. Phys.—JETP* **39** 920
[25] Rexford D G and Kim Y M 1972 *J. Chem. Phys.* **57** 3094
[26] Krätzig E and Kurz H 1976 *Ferroelectrics* **13** 295
[27] Meyer M, Schirmer O F and Pankrath R 2004 *Appl. Phys.* B **79** 395